On Fluid Compressibility in Switch-Mode Hydraulic Circuits - Part II: Experimental Results

James D. Van de Ven
Department of Mechanical Engineering
Worcester Polytechnic Institute
100 Institute Rd.
Worcester, MA 01609

E-mail: vandeven@wpi.edu
Phone: 508-831-6776
Fax: 508-831-5680

June 7, 2011
Revised: April 3, 2012

Abstract
In this paper, the author presents experimental work with a generic switch-mode hydraulic circuit that aims to validate a previously presented computational model, with primary focus on the energy loss due to fluid compressibility. While multiple previous papers have presented experimental works with switch-mode hydraulic circuits, the presented experimental system is unique due the capability of in-flow measurement of the entrained air in the hydraulic fluid and the bulk modulus of the fluid. A designed experiment was run that varied the entrained air, system pressure, and volume of the fluid experiencing pressure fluctuations, defined as the switched volume. The calculated volumetric efficiency from these experiments ranged from to 61% to 75%, with efficiency increasing with decreased levels of entrained air, system pressure, and switched volume. These efficiency trends and the pressure profile in the switched volume agree well with the computational model presented in part I of this two part set [1]. Differences between the experimental results and the computational model include approximately 10% higher predicted efficiency and pressure oscillations found in the experimental work that were not predicted by the model.

Keywords: switch-mode hydraulic circuit, digital hydraulics, compressibility experiments, bulk modulus

1. Introduction

As discussed in part I of this two part paper series [1], switch-mode hydraulic circuits enable an efficient, high bandwidth, ubiquitous, compact, and cost effective control method for hydraulic systems. While much research is focusing on the design of high-speed valves for switch-mode circuits, a gap existing in the understanding of the fluid compressibility in switch-mode circuits. In part I of this paper series, multiple bulk modulus models were discussed and a computational model was presented of the energy losses in a generic switch-mode circuit, with specific focus on the compressibility energy loss. In this follow-on paper, experimental work is presented that aims to validate the computational model and further explore physical phenomena related to compressibility in switch-mode hydraulic circuits.

Multiple previous works have performed experimental studies with switch-mode hydraulic circuits. Some of these works have utilized the experimental study to validate the pressure response predicted by a model, yet do not consider the energy losses or circuit efficiency [2-4]. Experimental work by Lumkes et al. with a custom valve in a pumping circuit yielded a measured efficiency of 49.5% at 20 Hz switching frequency and a duty cycle of 50%, yet the location and type of flow rate and pressure measurements used for the efficiency calculation were not specifically stated [5]. As will be done in this paper, the reported efficiency was the volumetric efficiency, which excluded other losses outside of the switch-mode portion of the circuit. Experimental work by Tu et al. with a pumping circuit resulted in measured efficiencies between 60-70% at 15 Hz switching frequency and a duty cycle of 60%. While the reported efficiency is also the

volumetric efficiency, the valve actuation power is also included in this calculation. For the efficiency calculation, the flow into the circuit was quantified by the angular velocity of the pump with the assumption of negligible leakage and the output flow was measured with a flow meter [6]. The author was unable to find any previous work with switch-mode circuits that measured the entrained air or bulk modulus of the fluid in the circuit, as is performed in this paper.

Multiple techniques have been developed for measuring the bulk modulus of a fluid including both direct and indirect methods. The present experiment imposes the requirement that the measurement method be applied to a continuously flowing fluid. This eliminates many of the direct measurement methods where a known volume of fluid is compressed by a piston or metal bellows and the change in pressure created by a change in volume is measured [7, 8], as these methods require a fixed volume of non-moving fluid. A direct in-flow measurement proposed by Watton compares the measured flow rate at two ends of a rigid conductor during a rapid change in pressure [9]. This approach is not suitable for the current application, as a steady inlet pressure is desired. A novel approach was presented by Kim and Wang based on the measured impedance of a piezoelectric transducer in the pressurized fluid [10].

Another approach to experimentally quantifying the bulk modulus, which is adopted in this paper, is to observe the velocity of a pressure wave in the fluid. This method utilizes the definition of the sonic bulk modulus:

$$\beta_e = \rho c^2 = \rho \left(\frac{L}{T} \right)^2 \tag{1}$$

where β_e is the effective bulk modulus, ρ is the mass density of the fluid, c is the velocity of sound in the fluid, L is the distance traveled by the pressure wave, and T is the time delay of the pressure wave [7, 11]. The sonic velocity approach was used by Yu et al., where a constant density, as obtained from the hydraulic fluid datasheet, was assumed [11]. Manring noted that this method is inconsistent with the definition of the bulk modulus where the density varies with pressure [12]. An attempt to address this issue was made by Cho et al. in their experimental results by computationally predicting the fluid density as a function of pressure based on the density at atmospheric pressure [13]. The approach used in this paper will measure the time delay of a pressure wave and utilized an average measured fluid density.

Following this brief introduction to the background of the problem, the experimental system design, system operation, and experiment design are presented in section 2. The results of the experiment, including power flows, calculated efficiency, and bulk modulus are presented in section 3. A discussion of the results is presented in section 4, followed by concluding remarks in section 5.

2. Methods

The goal of the experiment is to validate the computational model by studying the influence of circuit parameters that affect the compressibility energy loss on the volumetric efficiency. Specifically, the parameters varied in this study are the accumulator pressure, volume fraction of entrained air, and the volume of fluid experiencing pressure fluctuations, labeled the switched volume. To make the results of this work broadly applicable, a generic switch-mode motoring circuit will be considered using off-the-shelf components. The desired quantitative outputs from the experimental system are the efficiency of the circuit, defined as the hydraulic power out of the switched volume divided by the hydraulic power into the switched volume, and the effective bulk modulus.

This methods section is divided as follows. First, the design of the physical experimental system is presented, with focus on the measurement methods. Second, the system operation is discussed, including methods of data post-processing. Finally, the experiment design is presented.

Experimental System Design

The volume fraction of entrained air in the hydraulic fluid will be quantified in two ways. First, custom sight glasses, as seen in Figure 1, are used to visually observe air bubbles moving with the fluid flow. While the sight glasses do not provide a direct quantitative measure, they do provide qualitative results to support the density measurements while also providing information about the air bubble size distribution. Second, the density of the hydraulic fluid in the low-pressure portion of the circuit is measured and

compared to the density of vacuum degassed hydraulic fluid; any decrease in density at the same pressure can be attributed to entrained air. Numerous methods of measuring the fluid density in-flow were considered including measuring the buoyancy force on an object in the fluid, measuring the head pressure differential across a vertical tube, and measuring the mass of a known volume connected to the system through flexible conductors. Following marginal results with these methods, a coriolis mass flow meter capable of also measuring fluid density was employed. The meter has an advertised density measurement repeatability of ± 0.5 kg/m^3 and was factory calibrated immediately prior to the experiment. As the fluid density is also a function of temperature and pressure, the fluid temperature was maintained within a 6°C window during the experiments and the pressure at the coriolis flow meter was kept constant. It should be noted that this method allows calculation of the air volume fraction at low pressure. At high pressure the air will be compressed and an unknown quanity will dissolve in the hydraulic fluid.

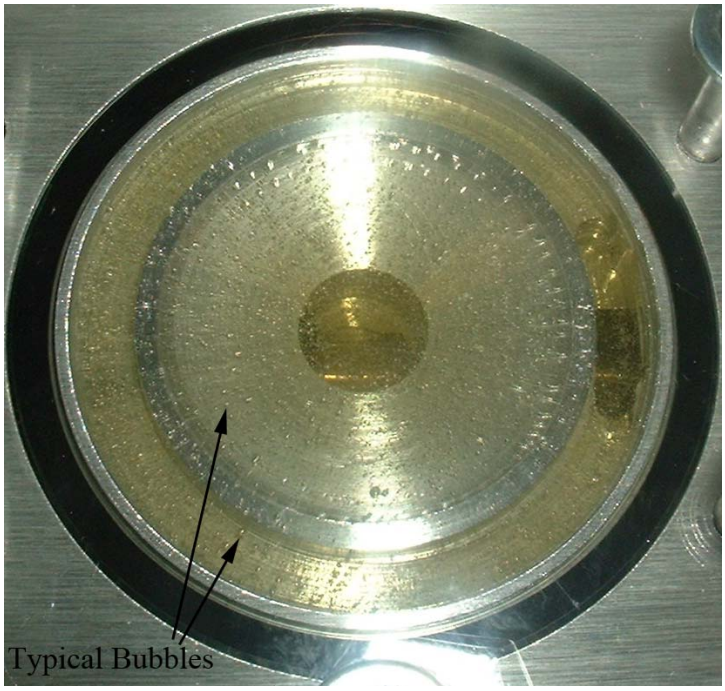

Figure 1. Photograph of the low-pressure sight glass at 3.1% entrained air by volume. Note the small diameter air bubbles entrained in the fluid.

Implementing the sonic velocity method of calculating the effective bulk modulus introduces unique requirements. First, a pressure wave source is required, which is readily available in a switch-mode circuit from the pulsatile flow through the switching valve. Second, the velocity of a pressure wave, which travels at approximately 1500 m/s in hydraulic fluid, must be accurately measured. For a 1.5 m distance between two pressure transducers, a time difference of 0.01 ms must be captured to observe a 1% difference in the effective bulk modulus. While the density of the fluid in the high-pressure branch of the circuit does change with the quantity of entrained air and the pressure, this change is quite small and within the noise of the measurement. For this reason, a constant fluid density was used in the sonic velocity bulk modulus calculation.

A schematic of the experimental system is presented in Figure 2. Starting from the left of the figure, pressurized air passes through a variable pressure regulator and a variable orifice and is injected into the hydraulic fluid at the inlet of the low-pressure hydraulic pump. The metered air and oil are pumped by a low-pressure pump through a sight glass and the coriolis flow meter, which measures mass flow and fluid density. The air enters the system through a 1 mm diameter orifice immediately before the inlet of the low-pressure pump to minimize air bubble size. The pressure in the low-pressure branch is controlled with a variable orifice returning to tank. The fluid in the low-pressure branch is pressurized by a variable-displacement high-pressure pump and then passes through a gear-style flow meter and the sonic velocity tube before reaching the accumulator, which is used to smooth the pressure ripples in the high-pressure rail.

The drain flow from the high-pressure pump is measured with another gear-style flow meter before it is returned to tank. The fluid in the accumulator section of the circuit enters the switch-volume through a three-way spool valve that is driven by a pulse-width modulated signal. Two additional entrances to the switched volume are from the low-pressure branch through the three-way valve and through the check valve. On the outlet of the switched volume is a gerotor motor, coupled to a flywheel, which provides inertia for the system. Finally, a load is applied to the circuit with a variable orifice after the hydraulic motor. Note that the arrangement of flow meters allows the flow rate through each flow path of the circuit to be calculated, while avoiding the pressure drop associated with a flow meter in the path from the low-pressure branch to the 3-way valve.

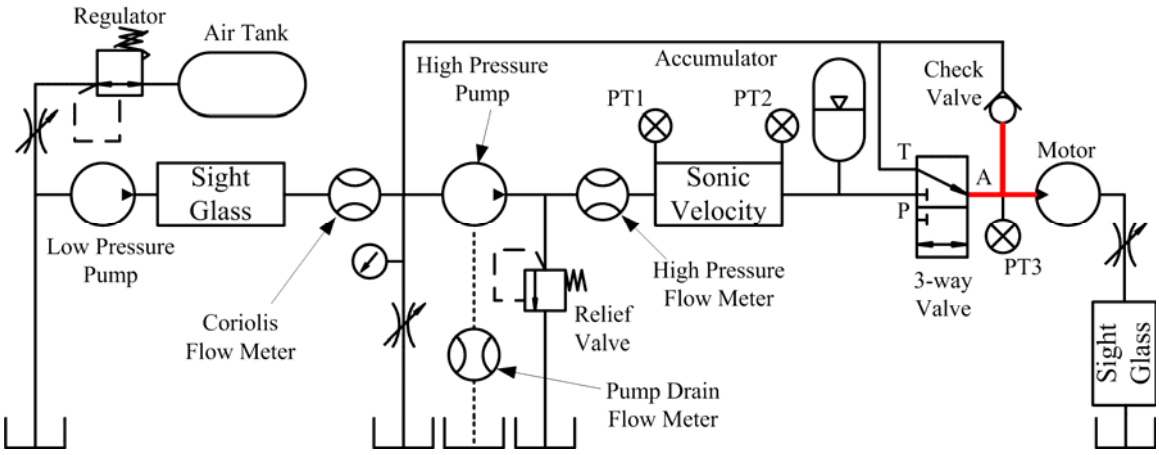

Figure 2. Schematic of the major components of the experimental system. The bold fluid volume between the 3-way valve and the motor is the switched volume.

As previously mentioned, to make the results of this work generally applicable to other systems, off-the-shelf components are used. Table 1 contains a list of the specifications of the major components critical to the switch-mode portion of the circuit. A picture of the physical system is provided in Figure 3. The 3-way valve was selected primarily based on the fast response time relative to other commercially available valves. To minimize the possibility of adding air to the hydraulic fluid after the low-pressure density measurement, a flooded-case axial piston architecture was chosen for the high-pressure pump. The hydraulic motor is designed for hydrostatic applications where the shaft seal can support pressure applied to both ports at the same time, as occurs in this circuit.

Table 1. Primary components used in the experimental system.

Parameter	Symbol	Value	Units
Switching Frequency	f	10	Hz
Duty Cycle	$Duty$	60	%
3-way Valve			
P→A Discharge Coefficient * Area	$C_D*A_{P\rightarrow A}$	$5.98\text{x}10^{-6}$	m^2
T→A Discharge Coefficient * Area	$C_D*A_{T\rightarrow A}$	$6.35\text{x}10^{-6}$	m^2
P→A Parallel Plate Leakage Coefficient	$k_{leak,P\rightarrow A}$	$1.85\text{x}10^{-15}$	m^3
P→A Parallel Plate Leakage Coefficient	$k_{leak,T\rightarrow A}$	$3.68\text{x}10^{-15}$	m^3
Transition Time: transition to P→A	t_P	12	ms
Transition Time: transition to T→A	t_T	22	ms
Check Valve			
Cracking Pressure	P_{crack}	20.7	kPa
Discharge Coefficient * Area	C_D*A_{check}	$7.375\text{x}10^{-6}$	m^2
Switched Volume	V_{switch}	10 - 42 (adjustable)	cm^3
Motor Displacement (Gerotor)	D	3.572	cm^3/rev
Flywheel Mass Moment of Inertia	I	0.0207	rad/s
Mass Density of Oil	ρ	876	kg/m^3
Dynamic Viscosity of Oil	η	0.0404	Pa*s
Bulk Modulus of Air Free Oil	β	1.9	GPa
Ratio of Specific Heats for Air	γ	1.4	unitless
Accumulator Pressure	P_{high}	4.1 - 6.9 (adjustable)	MPa
System Low Pressure	P_{low}	202	kPa
Atmospheric Pressure	P_o	101	kPa
Accumulator Volume	V_{accum}	0.473	liters
Accumulator Gas Precharge Pressure	P_{charge}	3.4	MPa

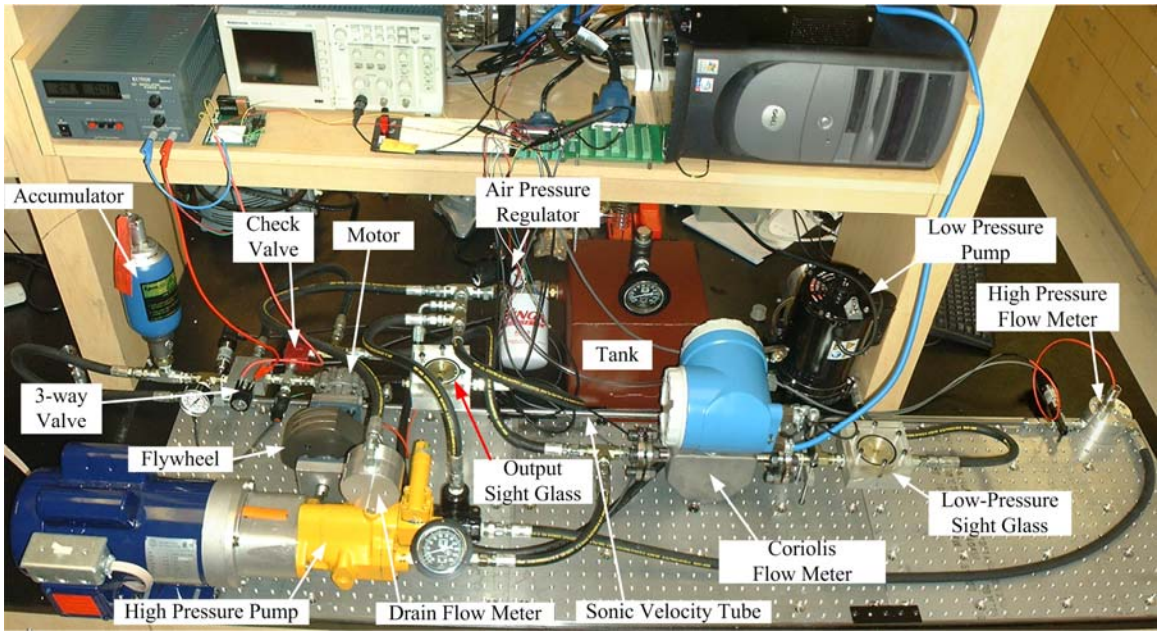

Figure 3. Photograph of the experimental system. Note, the switched volume between the 3-way valve and the motor is currently at the smallest volume, 20 cm^3.

System Operation

A set of operating parameters were developed to provide repeatable test results. First, the volume of the switched volume was set by adding or removing rigid fluid connectors. Second, all components of the

system were turned on and run for 20 minutes to allow the hydraulic fluid to reach operating temperature and the amplifying circuits to reach steady-state temperature. For all experiments, the hydraulic fluid temperature was maintained between 46°C and 52°C, as measured at the oil filter before the fluid returned to tank.

To start an experimental trial, the accumulator pressure was set to the desired value by adjusting the pressure compensation screw on the high-pressure pump. Next, the flow rate in the high-pressure rail, as measured by the high-pressure flow meter, was set to 2.85 liters/min by adjusting the load orifice after the hydraulic motor. The pressure in the low-pressure branch was then set to an absolute pressure of 202 kPa by adjusting the variable orifice that connects the inlet of the high-pressure pump to tank. Finally, the air volume fraction in the low-pressure branch, as quantified by the density measured with the coriolis meter, was set by adjusting the air pressure regulator and inlet orifice area. Typically, a second round of fine tuning each parameter was also necessary. Once conditions were stable, ten seconds of data were captured. The sampling rate of the three pressure transducers was set to a frequency of 100 kHz and the sampling rate of the other sensors was set to 10 kHz.

Data from the sensors was acquired using two data acquisition cards and then post-processed. First, the ratiometric signals were scaled based on the measured input voltage and then converted to appropriate units of pressure or density using linear calibration parameters. Next, the frequency output data of the coriolis and gear style flow meters were converted to flow rates by calculating the average period between pulses and using the calibration constants. The rising and falling edges of the pressure in the switched volume were detected by comparing the pressure to a threshold value, allowing calculation of the switching period and effective duty cycle. In Figure 4, the valve command and the pressure in the switched volume are plotted as a function of time; the markers on the pressure plot depict the rising and falling edge detection. From this plot, it is interesting to note the significant delay between the valve command signal and the start of a change in pressure. The observed time delay is the reason for limiting the switching frequency to 10 Hz for this off-the-shelf valve. These time delays of 23 ms to connected the pressure to switched volume ports and 14 ms to connect the tank and switched volume ports agree reasonable well with the transition time provided by the manufacturer, found in Table 1.

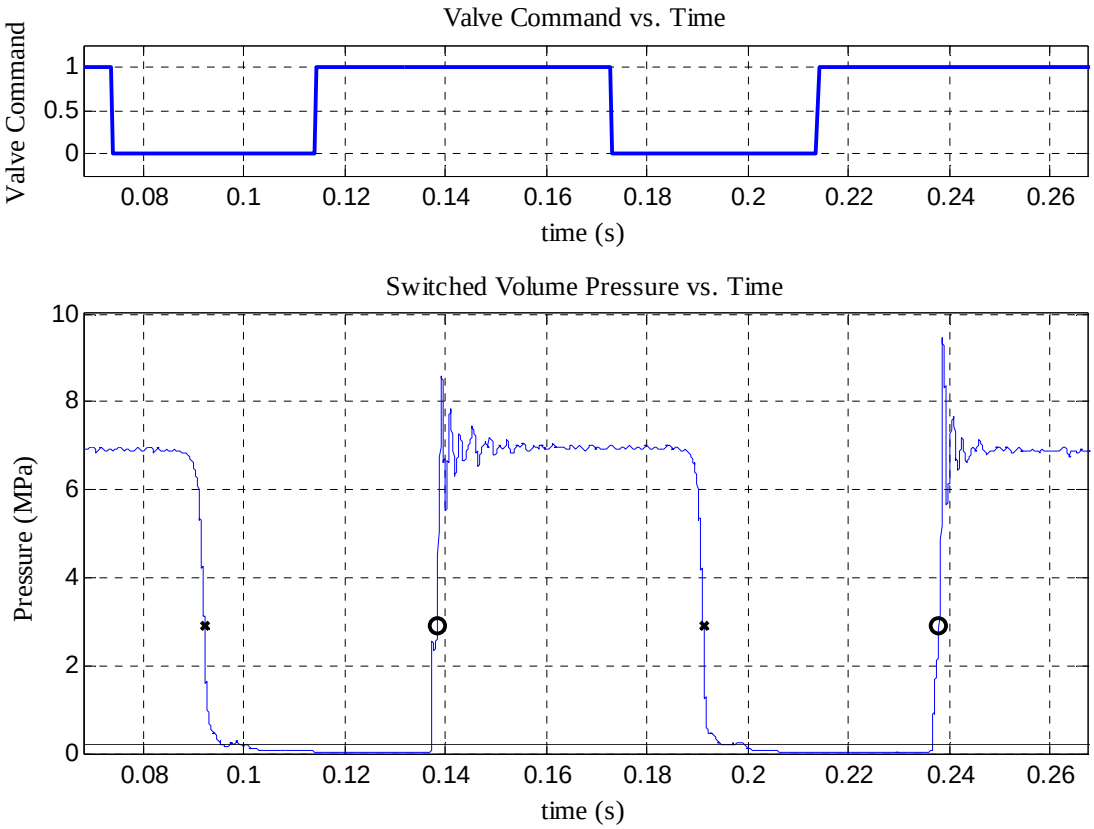

Figure 4. Valve command and pressure in the switched volume with a switching frequency of 10 Hz and a duty cycle of 60%. Note the detected rising and falling edges used to find the period and duty cycle. The horizontal line at 142 kPa corresponds to the pressure where the check valve opens. These data are for a 20 cm^3 switched volume, 6.9 MPa accumulator pressure, and air volume fraction of 2.5%.

The time-of-flight measurement for the sonic velocity bulk modulus calculation is complicated by the fact that there are three primary sources of pressure waves in the high-pressure branch. First, the axial piston pump creates pressure waves due to the sinusoidal displacement of each piston; these waves travel in the downstream direction through the sonic velocity tube. Second, the gear-architecture flow meter, located immediately before the sonic velocity tube, creates additional pressure waves that travel in the downstream direction. Third, the switching of the 3-way valve creates large magnitude pressure waves that travel in the upstream direction. To isolate the pressure wave created by the valve, a short sampling window is used immediately following the rising edge of the pressure in the switched volume, corresponding to the valve opening. To find the time delay of the pressure wave, the cross-correlation of pressure data at each end of the sonic velocity tube is used. The original data and time-shifted data for a typical event are presented in Figure 5. Note that the circle of the left side of the plots denotes the time of the rising edge of the pressure in the switched volume. Using the calculated sonic velocity, the effective bulk modulus is calculated from Eqn (1).

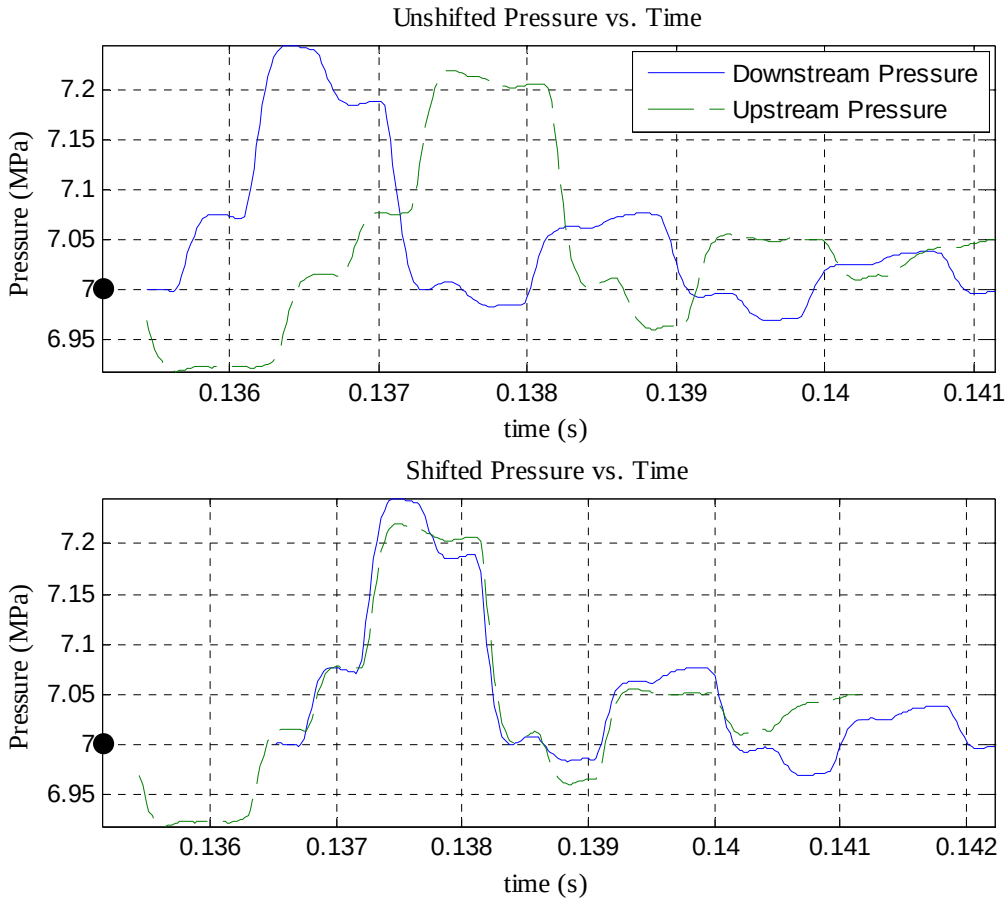

Figure 5. The top plot is the pressure at both ends of the sonic velocity tube after applying a low-pass filter with a 5 kHz cutoff frequency. The bottom plot shows the upstream data shifted by the 1.080 ms delay time, found from the maximum of the cross-correlation. The circle on the left of the plot is the time of the rising edge of the pressure in the switched volume.

Multiple forms of power need to be included in the calculation of the switch-mode circuit efficiency. In order to make the results of this work widely applicable, only the volumetric efficiency of the switch-mode circuit is considered, while the power losses of other components such as the pump, motor, or valve actuation are disregarded. While part I of this paper series focused on transient power loss [1], the slow response time of the gear flow meters neccesitates calculating the steady-state power for the experimental data. The primary source of power into the switch-mode portion of the circuit is the high-pressure flow from the accumulator:

$$Power_{hyd,HP} = \left(P_{accum} - P_{tank}\right) Q_{HP} \tag{2}$$

where $Power_{hyd,HP}$ is the high pressure hydraulic power, P_{accum} and P_{tank} are the pressure at the hydraulic accumulator and the tank respectively, and Q_{HP} is the volumetric flow rate through the high-pressure flow meter. Similarly, when the 3-way valve is in transition or connecting the T and A ports, flow enters the switched volume through the check valve and/or the 3-way valve from the low-pressure branch. This low-pressure hydraulic power is:

$$Power_{hyd,LP} = \left(P_{low} - P_{tank}\right)\left(Q_{coriolis} - Q_{drain} - Q_{HP}\right) \tag{3}$$

where P_{low} is the pressure in the low-pressure branch and $Q_{coriolis}$ and Q_{drain} are the volumetric flow rate through the coriolis meter and drain flow meter. Note that using the difference of the flow rate measured at the coriolis meter, pump drain, and high-pressure branch to calculate the flow through the check valve

assumes that the density of the fluid is constant, which is not strictly correct. However, the magnitude of this power into the system is small, making this assumption acceptable.

The final input power to the switch-mode circuit is the expansion of the entrained air from the high-pressure fluid. Assuming adiabatic expansion of the compressed air, the stored energy is:

$$E_{comp} = \int P(V)\,dV = P_{accum} V_{air,HP}^{\gamma} \int_{V_{air,HP}}^{V_{air,tank}} dV \Big/ V^{\gamma} = \frac{V_{air,HP}\left(P_{accum}^{1/\gamma} P_{tank}^{1-1/\gamma} - P_{accum} \right)}{1-\gamma} \tag{4}$$

where $V_{air,HP}$ and $V_{air,tank}$ are the volume of air at high pressure and tank pressure respectively and γ is the ratio of specific heats for air. The volumetric fraction of entrained air in the hydraulic fluid at low pressure is found from the density measurement of the coriolis meter, as earlier discussed. By assuming adiabatic compression of the entrained air from low pressure to high pressure, the air volume fraction at high pressure can be calculated. Finally, the air flow rate is found by multiplying this high-pressure air volume fraction by the flow measurement from the high-pressure flow meter, yielding a high pressure air volume of:

$$V_{air,HP} = \frac{V_{HP}}{\left(\frac{1}{R_{low}} - 1 \right) \frac{P_{accum}^{1/\gamma}}{P_{tank}^{1/\gamma}} + 1} \tag{5}$$

where V_{HP} is the volume of fluid at high pressure and R_{low} is the fraction of entrained air at tank pressure. Note that using the air fraction at low pressure to calculate the air fraction at high pressure neglects the increase in air absorption in the oil with increased pressure. Again, the magnitude of the power from the compressed air is small, making this assumption acceptable. The power, instead of the energy, associated with compressed air in the high-pressure fluid is calculated by using the time rate of change of Eqn (4).

The output power from the switched volume is absorbed by the pressure drop across the variable orifice after the motor. The instantaneous output power is found from:

$$Power_{out} = \left(P_{switch} - P_{tank} \right)\left(Q_{coriolis} - Q_{drain} \right) \tag{6}$$

where P_{switch} is the pressure in the switched volume. Because the pressure in the switched volume is constantly changing, as shown in Figure 4, the average output power is used to calculate the system efficiency. Finally, the switch mode circuit efficiency is:

$$\eta = \frac{Power_{out}}{Power_{in}} = \frac{Power_{out}}{Power_{hyd,HP} + Power_{hyd,LP} + Power_{comp}}. \tag{7}$$

Experiment Design

An experiment was designed to determine the influence of accumulator pressure, entrained air, and switched volume on the circuit efficiency. The system pressure was varied in three levels including 4.1 MPa, 5.5 MPa, and 6.9 MPa. Higher pressures were not explored due to the backpressure limitations of the hydraulic motor. Entrained air was allowed into the system through a needle valve at the inlet to the low-pressure pump. The air fraction by volume was varied across three levels: 2.5%, 3.1%, and 5.3%. Because the air level was calculated from the measured density in the low-pressure branch, the levels represented the entrained air fraction by volume at 202 kPa, not atmospheric pressure. The switched volume was varied in three levels including 20 cm^3, 30 cm^3, and 42 cm^3. The change in volume was achieved by adding rigid fluid connectors between the 3-way valve and the motor. Three replications were performed of each of the 27 factor level combinations, for a total of 81 samples.

The 81 experimental trials were all run in a single day to minimize day-to-day variation. Because changing the volume of the switched volume requires shutting down the system and changing fluid conductors, the three volume levels were run in batches. In addition, when higher air levels were reached, the system needed settling time to allow the entrained air to escape to the surface. Due to this fact, the air levels for each volume level were run sequentially from low air to high air. Within each air and volume factor combination, the replications of the three trials of the three pressure levels were randomized. For all

experiments, the switching frequency was set to 10 Hz and the duty cycle of the valve command was set to 60%.

3. Results

When running the experiment, the behavior of the system was qualitatively different with varying levels of air. At low levels of air, the system was very stable and setting and the desired flow and pressure was easily established and maintained. As the quantity of air increased, surges were observed in the flow rate through the high-pressure branch, making it more challenging to set and maintain the desired pressure and flow rate for an experimental trial. The sight glasses provided good visualization of the nature of the entrained air. In the low-pressure branch, the air bubble size was quite uniform with an estimated average diameter of 0.1 mm, as seen in Figure 1. The sight glass after the hydraulic motor and load orifice demonstrated even smaller bubble diameters as the air dissolved in the hydraulic fluid came out of solution. At 5.3% air volume fraction, a near-foaming behavior was observed in the output sight glass.

Before presenting the circuit efficiency, the individual power components will be presented. The output power, averaged for the three replications of each factor level combination, is shown in Figure 6. Recalling that the flow through the high-pressure branch is the same for all experimental trials, the output power has a strong dependence on the accumulator pressure and a lesser dependence on the entrained air and switched volume.

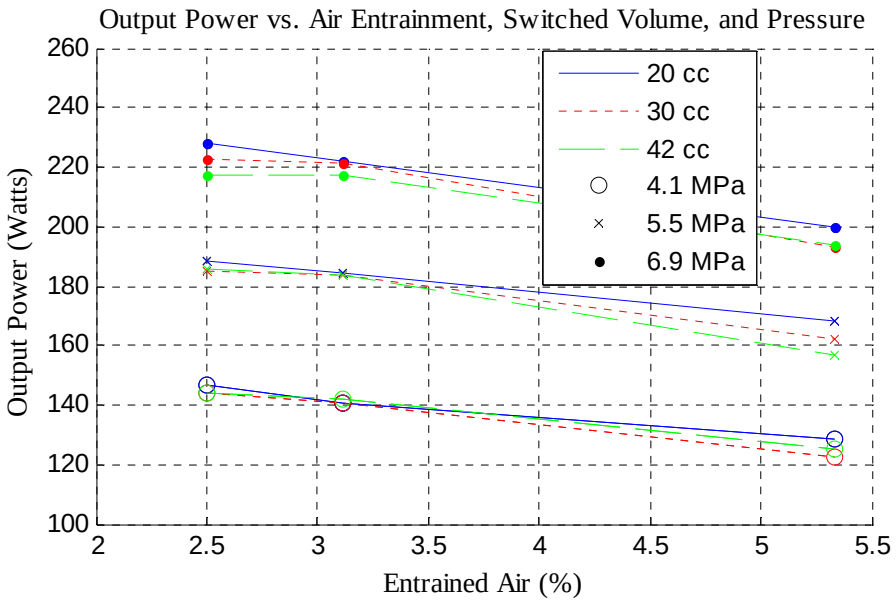

Figure 6. Output power as a function of entrained air, switched volume, and accumulator pressure.

To better understand the individual contributions of the different forms of input power, each form is separately presented. Both the high-pressure hydraulic power and air compressibility power are non-dimensionalized by dividing the individual input power by the output power. The non-dimensional values of these two input powers are presented in Figure 7. Note that the input power from the high-pressure branch is two orders of magnitude larger than compressed air input power. Because the input pressure of the low-pressure input power remains constant, the dimensional power is presented in Figure 8. For reference in comparison to Figure 7, in the non-dimensional form, the low-pressure input power varies from 0.003 to 0.012.

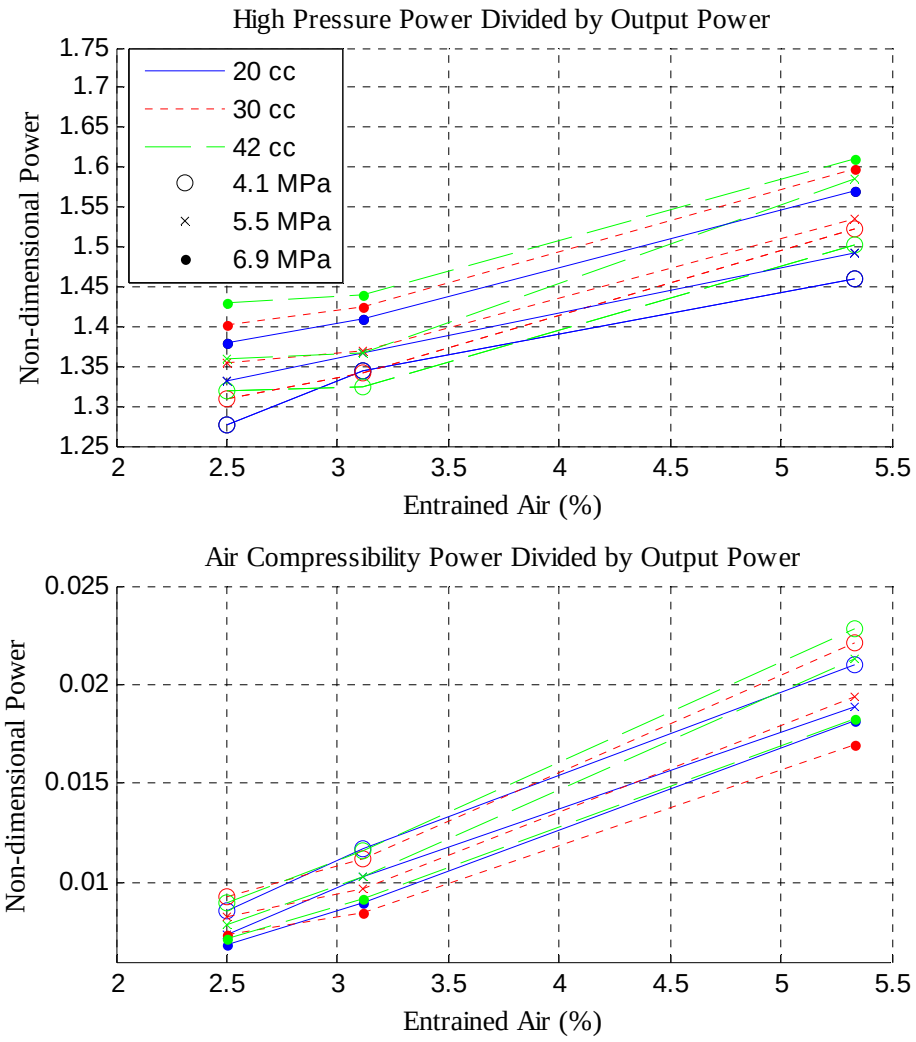

Figure 7. Non-dimensional high-pressure and compressed air power into the switched volume as a function of entrained air, switched volume, and pressure. The input powers are non-dimensionalized by dividing them by the output power.

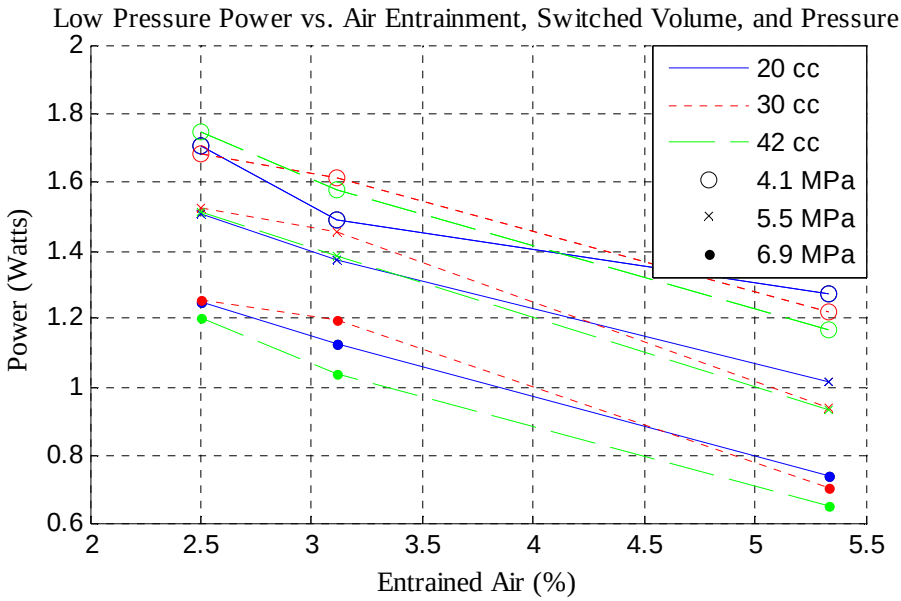

Figure 8. Input power from the low-pressure branch through the 3-way valve and the check valve.

From the above power data, the volumetric efficiency can be calculated. The volumetric efficiency, averaged for each factor level combination, is presented in Figure 9. The standard error for all of these data points is less than 0.6%.

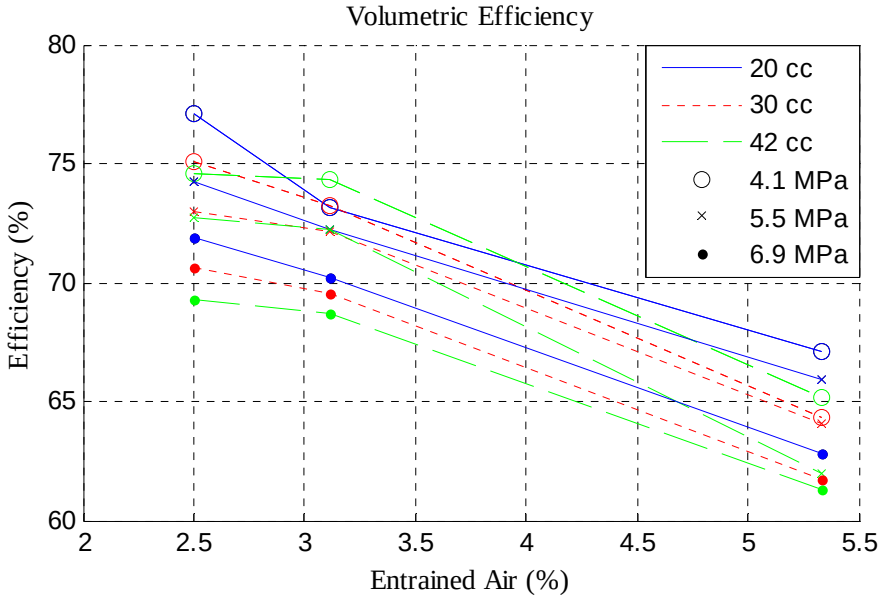

Figure 9. Volumetric efficiency as a function of the entrained air, switched volume, and accumulator pressure.

The last result of the experiment is the effective bulk modulus, which was calculated from the time-of-flight of the pressure wave through the sonic velocity tube. The effective bulk modulus, presented in Figure 10, is the average value across all volume levels and replications. Note that an additional entrained air fraction of 1.8% is added to see a broader view of the overall trend. This low air level represents the average measured air fraction when no air was added to the system. This level was not included in the above power and efficiency data as the entrained air increased with operating time and thus was not repeatable.

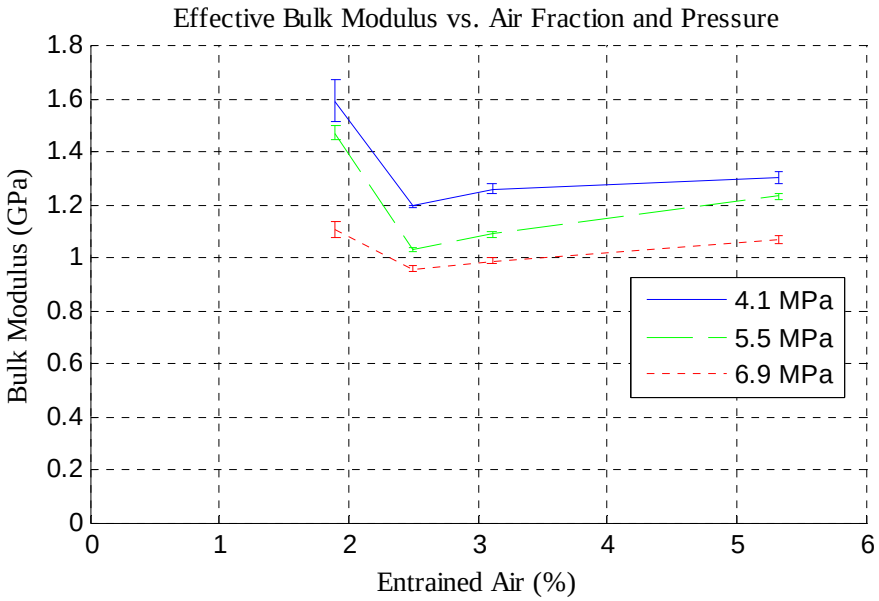

Figure 10. Effective bulk modulus as calculated by the sonic velocity method. The error bars are the standard error of the mean.

4. Discussion

The results of this experimental study provide meaningful results about the influence of switch-mode circuit parameters on the circuit efficiency and behavior. Foremost, the experimentally measured efficiency, Figure 9, and the efficiency predicted by the computational model, Figure 7 of part I of the paper series [1], follow the same trend where the efficiency decreases with increased levels of entrained air, switched volume, and pressure. A notable difference in the overall trend is that the model predicts a much larger influence of the switched volume on the efficiency than was observed in the experimental work. Beyond the trends, the computational model predicted higher efficiency than was observed experimentally, across all factor level combinations. As will be discussed below, the output power calculated for the experimental results is lower than the actual results, which results in lower calculated efficiency than the actual value. Beyond the error in the output power calculation, other possible sources of error include incorrect prediction of the valve opening and closing time and additional physical phenomena not included in the model.

The method of calculating the output power involved the assumption that the hydraulic motor and flywheel provide sufficient inertia that the output flow rate is constant, and not a function of the fluctuating pressure. From an energy analysis of the kinetic energy in the flywheel as a function of the torque pulses created during each switching event, the motor shaft speed varies up to 5% at the maximum pressure level. It does need to be noted, that for higher switching frequencies, a lower flywheel inertia is required to maintain the same coefficient of fluctuation in the shaft speed. The validity of the constant flow rate assumption is further brought into question by the fact that leakage occurs through the gerotor motor, with the direction of the leakage continuously changing with the fluctuating pressure. These two factors result in the flow rate through the orifice to be higher than average at high pressure and lower than the average flow rate at low pressure. Thus, the output power is likely higher than calculated due to the discussed assumptions.

An alternative method of measuring the output flow rate would be to continuously measure the angular velocity of the hydraulic motor. This method would eliminate the measurement error created by assuming a constant shaft speed. However, this method would be more susceptible to error created by leakage across the motor and was thus not chosen.

The power input to the switch volume was strongly dominated by the high-pressure hydraulic power, which increased with entrained air, pressure, and switched volume, when quantified in the non-dimensional form.

The input power due to compressed air in the high-pressure branch was found to increase with entrained air and volume. It is interesting to note that the non-dimensional form of compressed air power decreased with pressure. This result is explained through Eqn (4), where the accumulator pressure is raised to the power of the reciprocal of the specific heat ratio. It does need to be noted that the compressed air power calculation does not account for air dissolving in the hydraulic fluid. The final input power, the hydraulic flow from the low-pressure branch, provides the smallest contribution, yet it is interesting to note that this input power increases with a decrease in pressure and entrained air. This same behavior was predicted in the computational model presented in part I of this paper series where a flow reversal was observed from the switched volume to the tank port [1].

Observation of the pressure in the switched volume as a function of time provides evidence of the existence of additional physical phenomena in the physical system that was not included in the model. The experimentally measured pressure in the switched volume, as seen in Figure 4, exhibits large amplitude pressure oscillations when ramping up to high pressure, which were not predicted in the computational model, seen in Figure 5 of part I of the paper series [1]. The amplitude and frequency of this pressure oscillation is a function of the "stiffness" of the fluid in the switched volume, evident when comparing the pressure profiles of a low air and volume case, as seen in Figure 4, with a high air and volume case, as presented in Figure 11. While the pressure oscillations were not predicted by the model, a comparison of the two plot of the experimentally measured pressure with Figures 5 and 8 from the computational paper shows that the increase in time of the pressure fall with decreased fluid stiffness predicted by the model is observed in the experimental results.

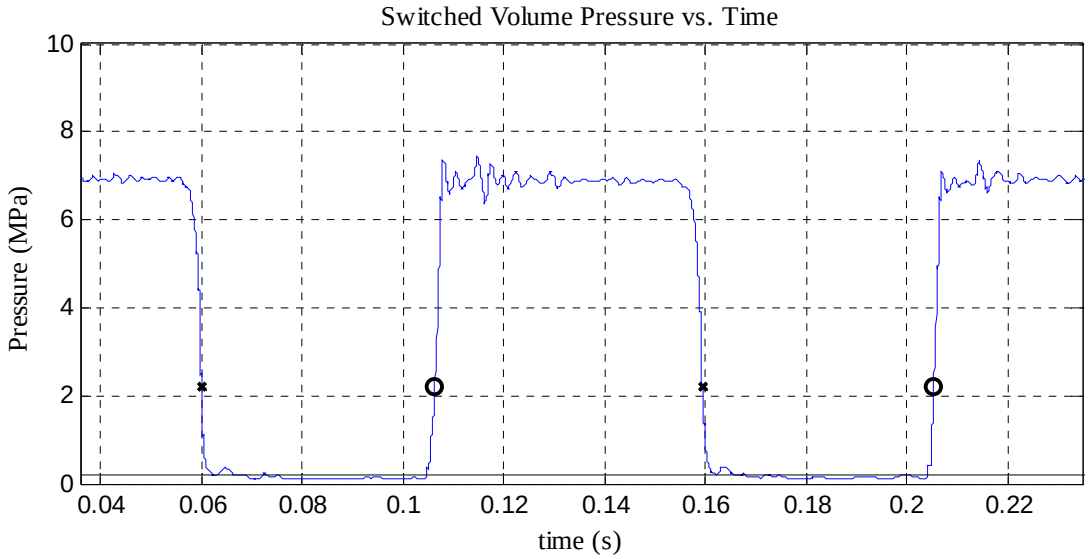

Figure 11. Pressure in the switched volume with a switching frequency of 10 Hz, a duty cycle of 60%, a switched volume of 42 cm^3, an accumulator pressure of 6.9 MPa, and an air volume fraction of 5.3%.

In contrast to the other results, the bulk modulus measured from the experimental results did not agree well with the predicted behavior. All models of the effective bulk modulus presented in part I of the paper series [1], predict an increase in bulk modulus with an increase in pressure or a decrease in entrained air. The bulk modulus experimentally measured with the sonic velocity method demonstrates a decrease with increased pressure. The role of entrained air on the experimental bulk modulus is unclear as the three air levels used for the power and efficiency results demonstrate an increase in bulk modulus with air level, while the bulk modulus at 1.8% entrained air level is significantly higher than the other three levels. The setup of the experimental system is likely the primary source of error leading to this result. Directly upstream of the sonic velocity tube was the gear-style high-pressure flow meter. When the pressure waves from the valve traveled upstream through the sonic velocity tube, there was likely reflection when the pressure waves contacted the flow meter. The magnitude and time of flight of these reflections would be higher for the low air and high-pressure cases, as observed in the pressure oscillation in the switched

volume. Additionally, the average degassed density was used in the effective bulk modulus calculation. Utilizing a measured density at pressure would provide a more accurate result.

5. Conclusion

The experimental study presented in this paper explored the influence of fluid compressibility on the efficiency of a generic switch-mode circuit operating at 10 Hz switching frequency and controlling a hydraulic motor. As predicted by the computational model presented in part I of the paper series [1], the volumetric efficiency of the experimental system decreased with increased levels of entrained air, accumulator pressure, and switched volume. The highest calculated efficiency of 75.4% was observed at 2.5% entrained air by volume, 4.1 MPa accumulator pressure, and 20 cm^3 switched volume. For reference, this is approximately 10% lower than predicted by the computational model. This discrepancy is likely due to the method of computing the output power, which does not account for variations in output flow with pressure in the switched volume, as occurs due to motor shaft speed variation and leakage across the motor.

Due to the desire to use off-the-shelf components to improve the generality of the work, the switching frequency was limited to 10 Hz. Multiple valves for switch-mode circuits are currently under development for switching frequencies of 20-100 Hz, or faster. As the compressibility energy loss occurs during each switch, these higher frequency systems will see a stronger influence of fluid compressibility than observed in this work.

It must be noted that the measured entrained air in the experimental system was in the low-pressure branch, which is at an absolute pressure of 202 kPa, not atmospheric pressure. Thus, the amount of air in the experimental system is higher than the same value in the computational model where the entrained air is quantified at atmospheric pressure. The elevated pressure in the low-pressure branch is required to prevent cavitation in the switched-volume that would otherwise occur due to the pressure drop from across either the tank to outlet port of the 3-way valve or the check valve. During tuning of the system, cavitation was observed audibly and visually by observing foaming of the hydraulic fluid in the sight glass after the load orifice. It is interesting to note that the entrained air fraction by volume varied from 1.6 to 2.2% when system reached steady operating conditions and no air was intentionally added to the circuit.

A major finding from the computational work is that the “stiffness” of the switched volume strongly influences the pressure profile in the switched volume, and thus the flow rates in the circuit [1]. At high levels of air, pressure, and volume, the fall time of the pressure in the switched volume decreased, as was predicted by the model. This behavior resulted in the power into the switched volume from the low-pressure branch decreasing with higher levels of air, pressure, and volume, likely due to a flow reversal as seen in the computational model. Unfortunately, these flow reversals could not be observed in the experimental system due to the measurement of the average, not continuous, flow rates. An additional phenomena seen in the experimental work that was not found in the model was oscillations in the pressure in the switched volume upon opening to the high-pressure branch. The frequency and amplitude of these oscillations increased with higher fluid “stiffness.”

The sonic velocity method was used to measure the in-flow effective bulk modulus of the fluid in the high-pressure branch. The results of these measurements were inconclusive and did not agree with the expected trends. A likely reason for this is that a free-stream flow did not exist upstream of the sonic velocity tube. Instead, a gear-style flow meter was directly upstream of the sonic velocity tube, which likely created reflection of the pressure waves that were traveling upstream from the switching action of the valve. There exists a need for an accurate, simple, and compact means of measuring the effective bulk modulus of a fluid while flowing through a circuit.

Beyond the need for bulk modulus measurement methods, an additional need of future work is the development of a model of fluid compressibility more applicable to switch-mode circuits than the bulk modulus. As discussed in part I [1], existing models do not consider the temperature and time dependence of air solubility nor the heat transfer time dependence of air compression and expansion. The developed computation model should account for these issues and be easy to experimentally measure for monitoring the performance of existing systems.

6. Acknowledgement
The author wishes to acknowledge John Taylor of Capella Technologies for constructing the sight glasses and technical assistance through multiple conversations regarding the behavior of an entrained gas in a liquid.

7. References
[1] Van de Ven, J. D., 2011, "On Fluid Compressibility in Switch-Mode Hydraulic Circuits - Part I: Modeling and Analysis," Journal of Dynamic Systems, Measurement, and Control(under review).
[2] Jeong, H.-S., and Kim, H.-E., 2002, "Experimental Based Analysis of the Pressure Control Characteristics of an Oil Hydraulic Three-Way On/Off Solenoid Valve Controlled by PWM Signal," Journal of Dynamic Systems, Measurement, and Control, 124, pp. 196-205.
[3] Li, P. Y., Li, C. Y., and Chase, T. R., "Software Enabled Variable Displacement Pumps," Proc. ASME International Mechanical Engineering Congress and Exposition, pp. 63-72.
[4] Tomlinson, S. P., and Burrows, C. R., 1992, "Achieving a Variable Flow Supply by Controlled Unloading of a Fixed-Displacement Pump," Journal of Dynamic Systems, Measurement, and Control, 114, pp. 166-171.
[5] Lumkes, J. H., Batdorff, M. A., and Mahrenholz, J. R., 2009, "Model Development and Experimental Analysis of a Virtually Variable Displacement Pump System," International Journal of Fluid Power, 10(3), pp. 17-27.
[6] Tu, H. C., Rannow, M., Wang, M., Li, P., Chase, T., and Van de Ven, J., 2011, "Design, Modeling, and Validation of a High-Speed Rotary PWM On/Off Hydraulic Valve," Journal of Dynamic Systems, Measurement, and Control(Under Review).
[7] Hayward, A. T. J., 1965, "The Compressibility of Hydraulic Fluids," Journal of the Institute of Petroleum, 51(494), pp. 35-52.
[8] Stern, H., 1997, "On the Bulk Modulus of Hydraulic Fluids in the Presence of Dissolved Gas," Fluid Power Systems and Technology, 4, pp. 113-123.
[9] Watton, J., 2007, Modelling, Monitoring and Diagnostic Techniques for Fluid Power Systems, Springer, London.
[10] Kim, G. W., and Wang, K.-W., 2009, "On-line Estimation of Effective Bulk Modulus in Fluid Power Ssytesm Using Piezoelectric Transducer Impedance," Journal of Intelligent Material Systems and Structures, 0, pp. 1-6.
[11] Yu, J., Chen, Z., and Lu, Y., 1994, "The Variation of Oil Effective Bulk Modulus with Pressure in Hydraulic Systems," Journal of Dynamic Systems, Measurement, and Control, 116, pp. 146-150.
[12] Manring, N. D., 1997, "The Effective Fluid Bulk-Modulus within a Hydrostatic Transmission," Journal of Dynamic Systems, Measurement and Control, 119, pp. 462-466.
[13] Cho, B.-H., Lee, H.-W., and Oh, J.-S., 2002, "Estimation Technique of Air Content in Automotic Transmission Fluid by Measuring Effective Bulk Modulus," International Journal of Automotive Technology, 3(2), pp. 57-61.